Nano Energy (2014) 8, 214–222

Available online at www.sciencedirect.com

ScienceDirect

journal homepage: www.elsevier.com/locate/nanoenergy

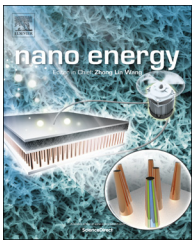

RAPID COMMUNICATION

One particle@one cell: Highly monodispersed PtPd bimetallic nanoparticles for enhanced oxygen reduction reaction

Jie Ying[a], Xiao-Yu Yang[a,*], Zhi-Yi Hu[d], Shi-Chun Mu[a], Christoph Janiak[c], Wei Geng[a], Mu Pan[a], Xiaoxing Ke[d], Gustaaf Van Tendeloo[d], Bao-Lian Su[a,b,**]

[a]*State Key Laboratory Advanced Technology for Materials Synthesis and Processing, Wuhan University of Technology, 122, Luoshi Road, Wuhan 430070, China*
[b]*Laboratory of Inorganic Materials Chemistry (CMI), The University of Namur (FUNDP), 61, rue de Bruxelles, B-5000 Namur, Belgium*
[c]*Institut für Anorganische Chemie und Strukturchemie, Heinrich-Heine-Universität Düsseldorf, 40204 Düsseldorf, Germany*
[d]*EMAT (Electron Microscopy for Materials Science), University of Antwerp, Groenenborgerlaan 171, B-2020 Antwerpen, Belgium*

Received 28 April 2014; accepted 10 June 2014
Available online 23 June 2014

KEYWORDS
PtPd nanoalloy;
Highly monodispersed nanoparticles;
Mesoporous materials;
Oxygen reduction reaction;
One particle@one cell structure

Abstract
Highly monodispersed platinum-based nanoalloys are the best-known catalysts for the oxygen reduction reaction. Although certainly promising, the durability and stability are among the main requirements for commercializing fuel cell electrocatalysts in practical applications. Herein, we synthesize highly stable, durable and catalytic active monodispersed PtPd nanoparticles encapsulated in a unique one particle@one cell structure by adjusting the viscosity of solvents using mesocellular foam. PtPd nanoparticles in mesocellular carbon foam exhibit an excellent electrocatalytic activity (over 4 times mass and specific activities than the commercial Pt/C catalyst). Most importantly, this nanocatalyst shows no obvious change of

*Corresponding author.
**Corresponding author at: State Key Laboratory Advanced Technology for Materials Synthesis and Processing, Wuhan University of Technology, 122, Luoshi Road, Wuhan 430070, China.
E-mail addresses: xyyang@whut.edu.cn (X.-Y. Yang), bao-lian.su@fundp.ac.be (B.-L. Su).

http://dx.doi.org/10.1016/j.nanoen.2014.06.010

structure and only a 29.5% loss in electrochemically active surface area after 5000 potential sweeps between 0.6 and 1.1 V versus reversible hydrogen electrode cycles.

Introduction

Platinum (Pt)-based nanostructures have been the most effective catalysts applied in proton-exchange membrane (PEM) fuel cells [1–5]. However, many critical issues must be addressed for the promise of their practical application, such as low cost, fast kinetics, high stability and durability [1,2,6,7]. There have been several successful routes to maximize the activity of a Pt-based catalyst by engineering its composites, morphologies and structures [8–10]. One of the techniques to improve the activity of cathode electrocatalysts and to reduce the content of Pt is the partial introduction of a secondary metal to alloy bimetallic Pt-based metals, e.g., PtPd, PtAu and PtAg [11–16]. Bimetallic nanostructured Pt-based metals do not only present the physicochemical properties of Pt, but also usually show a superior performance compared with pure Pt counterparts [17–19]. Significant progress has been subsequently made in the morphological and structural control of Pt-nanoalloy elctrocatalysts, for example, control of highly active facets and fabrication of branched structures [5,20–22]. The catalytic activity of bimetallic Pt-based nanoparticles can be greatly enhanced by maximizing the expression of active facets and/or sites toward a specific reaction. To further improve the stability, durability and utilization efficiency of metals, various types of nano-architectures, especially nanoporous structure, have been employed as catalyst support [23,24]. Large surface area of a nanoporous support facilitates the mass diffusion to improve the utilization efficiency of metals, and its pores partly prevent the aggregation and leaching of the metallic nanoparticles to enhance the stability and durability. For these reasons, the fine Pt-based nanoparticles supported on porous carbon are still the most commonly used electrocatalysts for the oxygen reduction reaction (ORR), such as commercial Pt/C. However, nanostructures applied on the metal nanoparticles have several deficiencies that need to be addressed before practical application. For example, the blocking of channels causes a decrease in surface area, and the aggregation of nanoparticles results in the irregularity of metal particles. It is therefore very necessary to synthesize uniform Pt-based bimetallic nanoparticles highly monodispersed in nanostructures for maximizing the activity of a Pt-based catalyst.

Most recently, synthesis strategies for nanoparticles dispersed in mesoporous materials have been developed to greatly improve the stability and durability of the nanoparticles. Successful approaches to monodispersed nanoparticles encapsulated inside mesostructured shells have been reported by Somorjai et al. and our group [25,26]. It is mostly important that each nanoparticle is uniformly dispersed inside each core@shell structure, which efficiently prevents aggregation of nanoparticles. These nanocatalysts therefore not only show high catalytic activity, but also feature high thermal-stability and durability.

Mesocellular foam with ultra-large mesoporous cells connected by meso-windows, having high thermal and hydrothermal stability, is a perfect template and support for the synthesis and encapsulation of nanoparticles [27–29]. Ideally, only one particle is uniformly dispersed inside one pore cell, which can minimize the aggregation of the nanoparticles and maximize the activity of the nanocatalysts. However, it seems impossible in traditional low-viscosity solvents (such as water [27], alcohol [28], and ethylene glycol [29]), because the random motion of the forming nanoclusters in low-viscosity solution, like Brownian motion [30], would results that the nanoparticles partly aggregate together or assemble in one cell. It has been known that such motion can be adjusted by altering the viscosity of the solvents. This phenomenon might be used to precisely control the growth of nanometals inside nanopores, nanocavities and nanochannels. Herein, we have successfully synthesized highly monodispersed PtPd bimetallic nanoparticles in the pores of MCF by adjusting the viscosity of the solvents. Very interestingly, each nanoparticle is uniformly encaged into each pore cell, showing a significantly superior eletrocatalytic activity and higher durability compared with the commercial Pt/C catalyst.

Experimental section

Materials synthesis

Mesocellular silica foam (MCF) was synthesized according to the published literature [31] and the mass ratio of Pluronic P123/HCl/1,3,5-trimethylbenzene/TEOS/H_2O is 1/2.2/0.75/2.2/37.5. Mesocellular carbon foam (MCF-C) was synthesized according to the published literature [32]. Mesocellular aluminosilicate foam (AlMCF) was first synthesized, with the molar ratio of MCF/$AlCl_3$/H_2O as 1/0.34/10. Then MCF-C was synthesized by using furfuryl alcohol as a carbon source, with the mass ratio of AlMCF/furfuryl alcohol as 1/2.25. In a typical synthesis of PtPd@MCF, 0.05 mmol Pt $(acac)_2$ (acac=acetylacetonate), 0.05 mmol $Pd(acac)_2$ and 1 mmol polyvinylpyrrolidone were added to 20 ml of 1,4-butanediol at room temperature under stirring. Then the solution was heated to 50 °C and 0.2 g MCF-Si was added to the solution. After stirring at 50 °C for 12 h, the mixture was heated to 215 °C under nitrogen atmosphere. After stirring at 215 °C (±2 °C) for 0.5 h, the mixture was cooled to room temperature in air and an excess of acetone was poured into the solution to form a suspension. After being filtered, washed, and dried, the final PtPd@MCF sample was obtained. PtPd@MCF-C and PtPd/C samples were synthesized under the same conditions, except that MCF was substituted by MCF-C and Vulcan XC-72 carbon.

Physical characterization

X-ray diffraction (XRD) patterns were collected using a Bruker D8 Advance X-ray diffractometer equipped with Cu Kα radiation. Scanning electron microscopy (SEM) experiments were performed using an S-4800 electron microscope (HITACHI, Japan). Transmission electron microscopy (TEM) images were carried out on a JEOL JEM-2100F microscope, operated at 200 kV in Wuhan University of Technology. High-angle annular dark-field scanning TEM (HAADF-STEM) and energy-dispersive X-ray spectroscopy (EDX) were carried out on a FEI Titan 80–300 "cubed" microscope fitted with an aberration-corrector for the probe forming lens, and four Brucker Quanta X EDX detectors, operated at 200 kV in University of Antwerp. The nitrogen adsorption and desorption isotherms at the temperature of liquid nitrogen were measured using a Micromeritics ASAP 3020 system. The samples were outgassed for 10 h at 200 °C before the measurements. The surface area was obtained according to the Brunauer–Emmett–Teller (BET) method. The pore size distribution was derived using the Barrett–Joyner–Halenda (BJH) model. The concentration of catalysts was determined by the inductively coupled plasma atomic emission spectroscopy (Optima 4300DV, Perkin Elmer Ltd., USA).

Electrochemical measurements

Cyclic voltammetry (CV) and ORR were carried out with a three-electrode system. A saturated calomel electrode was used as a reference electrode and platinum wire was used as a counter electrode. The loading amount of metal for the catalysts was 3 μg (i.e., 15.3 μg/cm^2 based on the geometric electrode area of 0.196 cm^2). To measure the electrochemically active surface area (ECSA) of catalysts, CV measurements were carried out in 0.1 M $HClO_4$ solutions under a flow of N_2 at a sweep rate of 50 mV/s. The ORR measurements were performed in 0.1 M $HClO_4$ solutions under flow of O_2 using the glassy carbon rotating disk electrode (RDE) at a rotation rate of 1600 rpm and a sweep rate of 10 mV/s. The accelerated durability tests were performed at room temperature in O_2-saturated 0.1 M $HClO_4$ solution by applying cyclic potential sweeps between 0.6 and 1.1 V versus RHE at a sweep rate of 50 mV/s for a given number of cycles.

Results and discussion

The overall synthesis procedure employed for the preparation of PtPd@MCF composites with one particle@one cell structure is illustrated in Figure 1a. Mixing and impregnation are performed with a defined amount of reaction precursor per MCF exo-template, and the precursors enter into the MCF channels by capillary interaction. During the thermal treatment, the reaction precursor is converted into metal nanoclusters in MCF. When the reaction solvent of the appropriate high-viscosity is used, highly uniform PtPd bimetallic nanoparticles inside MCF are formed. After washing, filtering and drying, PtPd@MCF with one particle@one cell structure is obtained. The surface morphologies and the detailed nanostructures of PtPd@MCF are illustrated by TEM (Figure 1b, c), HAADF-STEM (Figure 1d, e) and SEM (Figure S1) images. As shown in Figure 1b, a large number of nanoparticles are highly monodispersed in the cells of MCF. Figure 1c clearly shows that one particle is in one cell of MCF. The HAADF-STEM (Figure 1d and e) and SEM images (Figure S1a) show that the sample consists of uniformly sized, large spherical cells with a diameter of around 25 nm, and the cells are interconnected by uniform windows to create a continuous 3D pore system, which is in good agreement with the original MCF (Figure S1b). This reveals that the characteristic 3D mesocellular arrangement of the MCF frameworks could be retained after the incorporation of PtPd nanoparticles. Similar to the data of TEM, the well-dispersed nanoparticles are observed in the 3D interconnected porous structure. It is also notable that only one nanoparticle is encaged in one cell structure. Figure 2 shows the elemental mapping of one particle in the cell of MCF measured by HAADF-STEM energy-dispersive X-ray spectroscopy (HAADF-STEM-EDX). The results clearly demonstrate that the particle is a PtPd bimetallic nanoparticle, where Pt and Pd elements are randomly distributed throughout the whole nanoparticle. A high magnification HAADF-STEM image of a single particle further confirms the PtPd nanoparticle has a nanoalloying intermetallic structure with a good crystalline degree, but no atomic scale ordering between Pt and Pd (Figure S3). Meanwhile, the inductively coupled plasma-atomic emission spectrometry (ICP-AES) and TEM-EDX results show that the molar ratio between Pt and Pd is about 1:1, which is in good agreement with the Pt/Pd atomic ratio in the initial reaction mixture. This implies that all the Pt and Pd precursors are reduced in the reaction. These results suggest that the highly dispersed PtPd alloy nanocrystals could grow up inside the cells of the MCF. Very interestingly, most nanoparticles are individually encaged within a single cell. This one particle@one cell structure is a unique phenomenon that can prevent nanoparticles from aggregation and improve the utilization efficiency of nanometals, which is very crucial to PtPd nanoparticles in practical applications. The XRD patterns of the MCF and PtPd@MCF samples are shown in Figure S4. In case of the PtPd@MCF sample, the four observed peaks can be assigned to (111), (200), (220) and (311) planes of PtPd bimetal nanoparticles, and the broad peaks are due to the decrease in particle size of the bimetallic nanoparticles. The four diffraction peaks of the PtPd@MCF sample are slightly shifted to higher 2 theta values with respect to the corresponding peak of Pt (JCPDS no. 04-0802), suggesting contraction of the lattice parameters. This also reveals the alloy formation between Pt and Pd, which is caused by the incorporation of Pd in the fcc structure [33]. The retention of the well-defined MCF frameworks upon nanoparticle introduction is further confirmed by nitrogen adsorption-desorption data. The nitrogen adsorption-desorption isotherms and pore size distribution (inset) of MCF and PtPd@MCF samples exhibit a type IV characteristic and steep hysteresis of type H1 at high relative pressures (Figure S5), which is typical for mesoporous materials possessing large pore sizes with narrow size distributions [31,34]. The PtPd@MCF sample shows a high surface area (578 m^2 g^{-1}) and a large pore volume (2.22 cm^3 g^{-1}) (Table S1). Compared with the MCF sample, the surface area, pore volume, cell diameter and window diameter of the PtPd@MCF sample has slightly decreased, which is attributed to the embedded nanoparticles. This result suggests

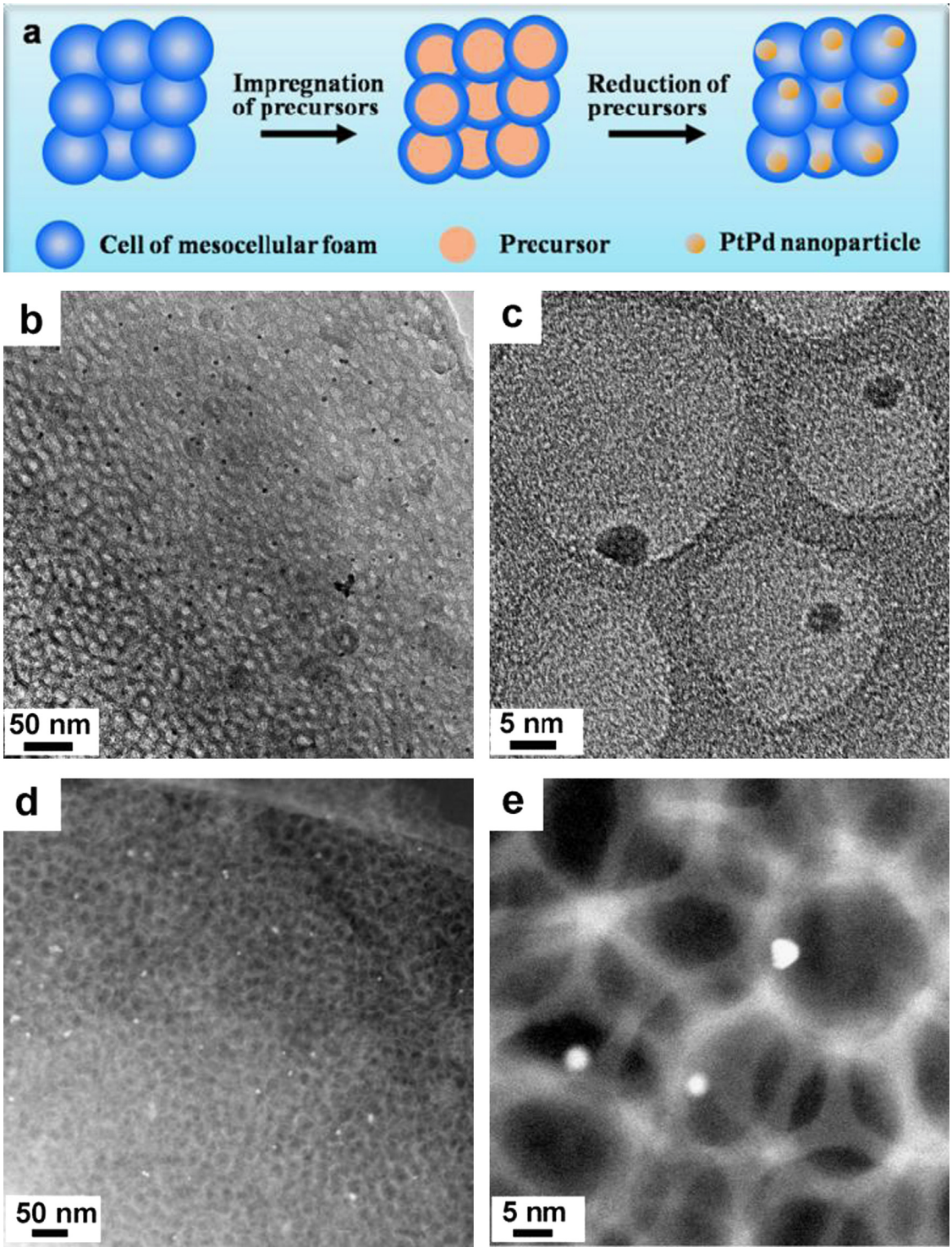

Figure 1 (a) Schematic representation of the preparation of PtPd@MCF sample. (b, c) TEM images of PtPd@MCF at low magnification and high magnification, respectively. (d, e) HAADF-STEM images of PtPd@MCF sample at low magnification and high magnification, respectively.

that PtPd nanoparticles have been immobilized inside the MCF pores, and do not block the channels.

To better understand the formation mechanism of this one particle@one cell structure, the role of the solvent in our reaction system was investigated. TEM images of PtPd nanoparticles in MCF synthesized in various solvents are shown in Figure S6. In ethylene glycol, the size of the aggregates is around 15 nm (Figure S6a), which are obviously formed by several small PtPd nanoparticles. It is also seen that dozens of small nanoparticles aggregate to form large sized particles (around 40 nm; Figure S6b) in water. Notably, the size of small nanoparticles in the aggregates synthesized

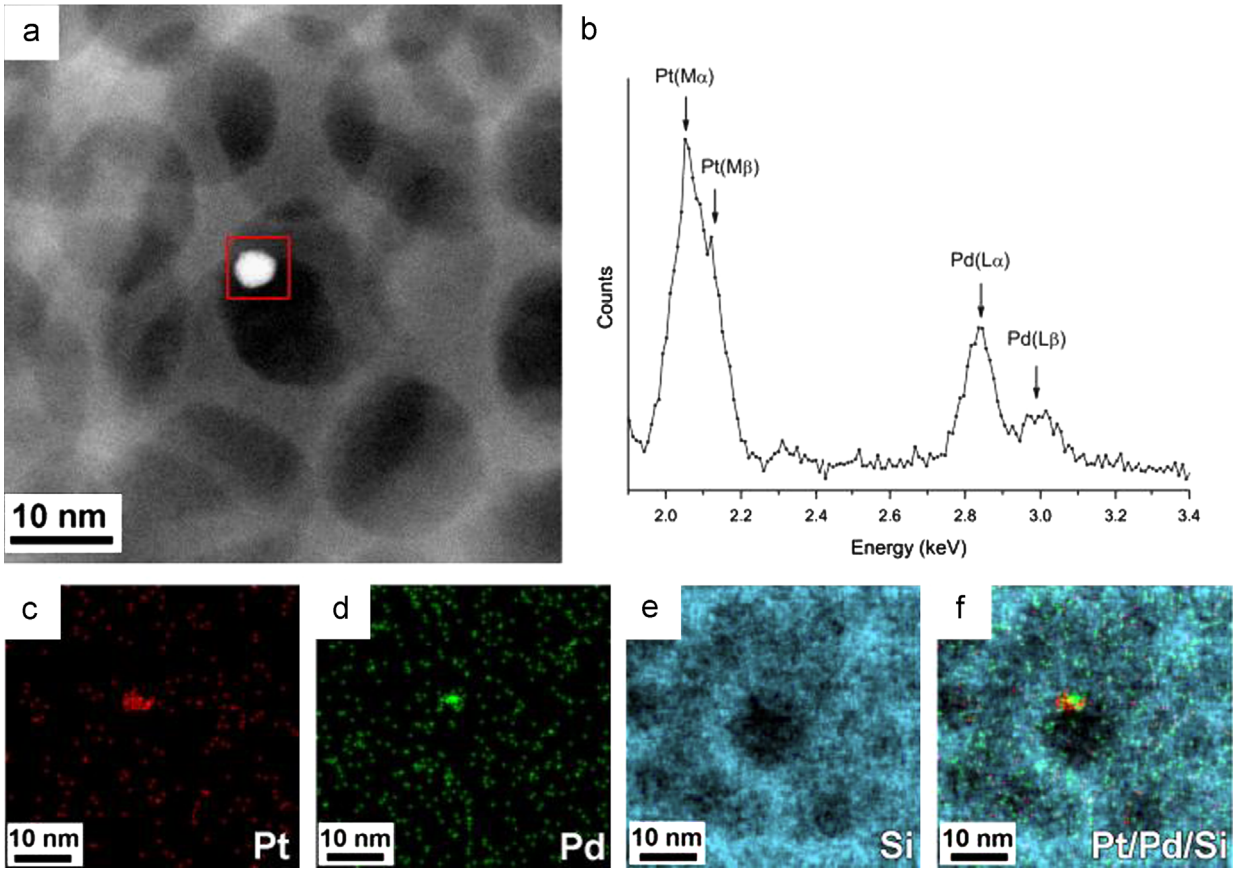

Figure 2 (a) High magnification HAADF-STEM image of PtPd@MCF sample. (b) Detailed EDX spectrum of the area indicated in (a). (c–f) EDX elemental mapping results: (c) Pt (red), (d) Pd (green), (e) Si (blue), (f) Pt, Pd and Si overlaid color mapping. Full EDX spectrum of (b) is included in Figure S2. (For interpretation of the references to color in this figure legend, the reader is referred to the web version of this article.)

in both ethylene glycol and water are around 5 nm, which is similar to the monodispersed PtPd nanoparticles synthesized in 1,4-butanediol. This means that the size of PtPd nanoparticles synthesized in various solvents is nearly identical. With decreasing solvent viscosity, the nanoparticles tend to aggregate. The largest aggregate is formed by dozens of single nanoparticles in the lowest viscosity solvent (water; 1.2 mPa s at room temperature) (Figure S6b). The viscosity of the solvent and the size of the particle/aggregation have an inverse relationship. For example, the ratio (1:2.7) of viscosity between ethylene glycol (21 mPa s at room temperature) and 1,4-butanediol (56 mPa s at room temperature) is close to the inverse ratio (3:1) of the particles size between aggregate synthesized in ethylene glycol (around 15 nm; measured by TEM) and 1,4-butanediol (around 5 nm; measured by TEM). The variation of the particle size is attributed to the viscosity variation of the solvent, because this is the most distinct difference in synthesis conditions between the nanoparticles synthesized in ethylene glycol and 1,4-butanediol. These results indicate that the viscosity of the solvent is a critical factor to control size and uniformity of metal nanoparticles, because viscosity of the solvent has a significant influence on the distribution of precursor in MCF channels before the formation of metal nanoparticles, the mobility of seed crystals during the formation of metal nanoparticles and stability of as-synthesized nanoparticles.

Due to their unique one particle@one cell structure, the PtPd@MCF sample is expected to exhibit high catalytic performance, especially in electrocatalytic applications. Thus, we evaluated the electrocatalytic properties of the PtPd nanoparticles encapsulated in electroconductive mesocellular carbon foam (designated as PtPd@MCF-C) against PtPd nanoparticles supported on Vulcan XC-72 carbon (designated as PtPd/C) and the commercial Pt/C catalyst (Figure 3 and Table S2). Figure 3a shows the CV curves of the samples recorded in N_2-purged 0.1 M $HClO_4$ solutions at room temperature with a sweep rate of 50 mV/s. Based on the CV curves, we calculated the ECSA by measuring the charge collected in the hydrogen adsorption/desorption region after double-layer correction and assuming a value of 210 $\mu C/cm^2$ for the adsorption of a hydrogen monolayer. The PtPd@MCF-C sample displays an outstandingly high ECSA of 72.6 m^2/g, which is higher than that of the PtPd/C and Pt/C catalyst. Figure 3b shows the ORR polarization curves of the catalysts performed in O_2-saturated 0.1 M $HClO_4$ solutions by using a glassy carbon RDE at room temperature with a sweep rate of 10 mV/s. As shown in Figure 3c, the PtPd@MCF-C and PtPd/C sample show a higher catalytic activity comparing to the commercial Pt/C, proving the advantage of alloying in electrocatalytic catalysis. Meanwhile, the PtPd@MCF-C sample exhibits a mass activity of 0.443 A/mg on the basis of the mass of Pt at 0.9 V versus RHE, which is about 4.4 times greater than that

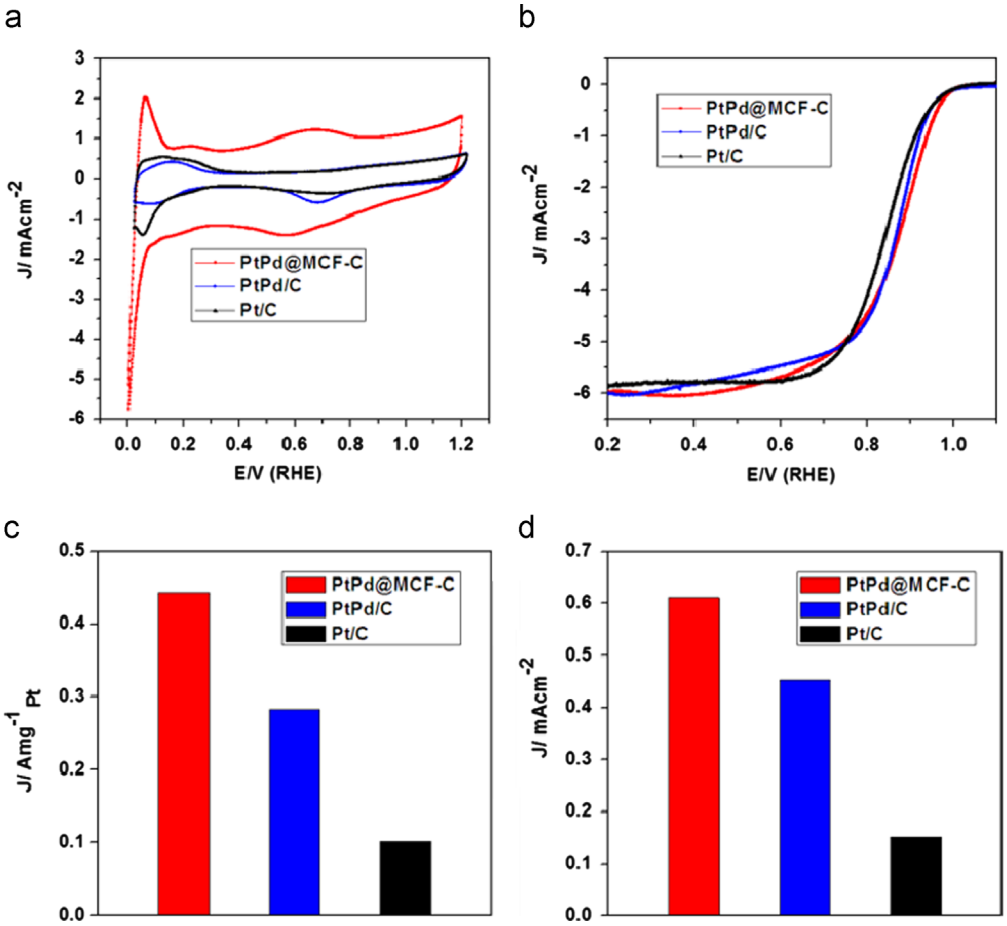

Figure 3 (a) Cyclic voltammetry (CV) curves, (b) ORR polarization curves, (c) mass activity and (d) specific activity at 0.9 V versus RHE for PtPd@MCF-C, PtPd/C and Pt/C catalysts.

of the Pt/C catalyst. The specific activities (i.e., kinetic current per unit area of catalyst) of the two catalysts also showed similar trends to that of the mass activities (Figure 3d). The PtPd@MCF-C sample (0.611 mA/cm^2) has a specific activity of about 4.0 times that of the Pt/C catalyst. Notably, the PtPd@MCF-C show desired structural superiority in electrocatalysis. For example, the mass activity of PtPd@MCF-C is 0.443 A/mg, while the mass activity of PtPd/C is 0.283 A/mg. The enhanced electrocatalytic activity of the PtPd@MCF-C sample should be ascribed to nanoalloying effect, 3D nanoarchitecture and highly desperation of nanoparticles in unique immobilization structure.

We also performed accelerated durability tests (ADTs) by applying linear potential sweeps between 0.6 and 1.1 V (vs RHE) at 50 mV/s in O_2-saturated 0.1 M $HClO_4$ solutions at room temperature. As shown in Figure 4 and Figure S7, the PtPd@MCF-C sample and commercial Pt/C catalyst show losses of 15.9% and 30.3% in ECSA after 2000 potential cycles, respectively. After 5000 cycles, the CV measurements show a loss of 29.5% in ECSA for the PtPd@MCF-C sample and 48.4% for the commercial Pt/C catalyst, revealing that the durability of the PtPd@MCF-C sample is also better than the commercial Pt/C catalyst. The high durability and stability of the PtPd nanoparticles in MCF-C can be reasonably attributed to the unique structure, which is further evidenced by TEM studies (Figure 4 inset a-d). The TEM image of the PtPd@MCF-C sample (Figure 4 inset a) shows that nanoparticles with a diameter of around 3 nm are highly monodispersed in the cells of MCF-C. Notably, the structure of each nanoparticle within each cell is clearly observed from the HRTEM image (Figure S8), which is very similar to the results of PtPd@MCF. This indicates that the alloyed PtPd nanocrystals could grow highly dispersed inside the cells of MCF-C. The TEM image of the commercial Pt/C catalyst (Figure 4 inset b) shows that Pt nanoparticles are highly monodispersed in the active carbon matrix and the size of the Pt nanoparticles is also around 3 nm (average size measured by TEM). After 5000 potential cycles, the dispersion and size of the PtPd nanoparticles in MCF-C show no obvious change (Figure 4 inset c), while severe aggregation was observed for the commercial Pt/C catalyst (Figure 4 inset d). This shows the great superiority of the "one particle@one cell" structure, and should be a direct reason of the high durability of the PtPd@MCF-C sample. Two features of the PtPd@MCF-C sample should contribute to the improved catalytic activity and durability: (1) 3D mesostructured supported materials not only provide a high surface area, but also make the PtPd nanoparticles less vulnerable to dissolution and aggregation during the growth and reaction; (2) the high dispersion of PtPd nanoparticles, especially each nanoparticle inside its own cell, not only

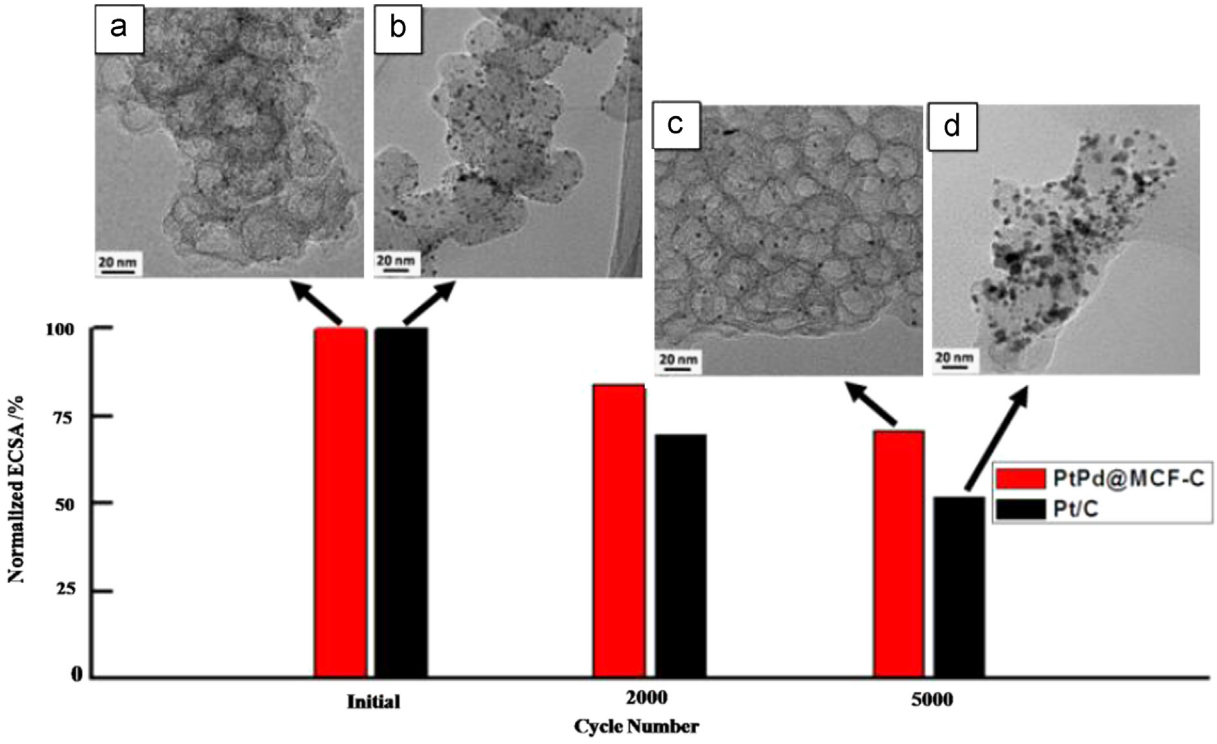

Figure 4 Loss of ECSA of PtPd@MCF-C (red left column) sample and Pt/C catalyst (black right column) after potential sweep cycles. Inset: TEM images of PtPd@MCF-C sample (a, c) and Pt/C catalyst (b, d) before and after 5000 potential sweeps cycles between 0.6 and 1.1 V at 50 mV/s in O_2-saturated 0.1 M $HClO_4$ solutions at room temperature. All scale bars in TEM images are 20 nm. (For interpretation of the references to color in this figure legend, the reader is referred to the web version of this article.)

prevents the aggregation of nanoparticles and improves the utilization efficiency of nanometals, but also maximizes the expression of active facets and/or sites of PtPd nanoparticles.

Conclusions

In summary, we have presented a facile process to synthesize a PtPd@MCF sample with a novel *"one particle@one cell"* structure. A viscosity-adjusting mechanism is proposed to explain the formation of the novel *"one particle@one cell"* structure. The PtPd@MCF-C sample shows high mass and specific activities that are 4.4 and 4.0 times greater than those of the commercial Pt/C catalyst. Most importantly, this nanocatalyst shows no obvious change of structure and enhanced durability after 5000 cycles. The synthesis approach described here is simple and general for the design of practical catalysts and nanoreactors [26], and can also be extended to the synthesis of other highly monodispersed metals [35], metal oxides [36], zeolites [37–39] and hybrids [40], which is expected to result in the discovery of new multifunctional materials allowing fascinating catalytic and other performances [41,42].

Acknowledgments

This work was supported by the Chinese Ministry of Education (NCET-11-0688, IRT1169, RFDP-20110143120006, 2012-YB-04, 2012-Ia-008), NFSC (51101115), NSFHB (2011CDB429) and SKLWUT (2013-ZD-6, 2011-PY-3). B.L.S. acknowledges "Program of Global Expert" and program of "Chang Jiang Scholar". X.Y.Y. acknowledges program of "Chutian Scholar". Z.Y.H., X.K. and G.V.T. acknowledge the ERC Grant no. 246791-COUNTATOMS.

Appendix A. Supporting information

Supplementary data associated with this article can be found in the online version at http://dx.doi.org/10.1016/j.nanoen.2014.06.010.

References

[1] Y. Bing, H. Liu, L. Zhang, D. Ghosh, J. Zhang, Chem. Soc. Rev. 39 (2010) 2184–2202.
[2] M.K. Debe, Nature 486 (2012) 43–51.
[3] A. Chen, P. Holt-Hindle, Chem. Rev. 110 (2010) 3767–3804.
[4] J. Wu, H. Yang, Acc. Chem. Res. 46 (2013) 1848–1857.
[5] B. Lim, M. Jiang, P.H. Camargo, E.C. Cho, J. Tao, X. Lu, Y. Zhu, Y. Xia, Science 324 (2009) 1302–1305.
[6] F. De Bruijn, V. Dam, G. Janssen, Fuel Cells 8 (2008) 3–22.
[7] H.A. Gasteiger, N.M. Marković, Science 324 (2009) 48–49.
[8] L. Zhang, R. Iyyamperumal, D.F. Yancey, R.M. Crooks, G. Henkelman, ACS Nano 7 (2013) 9168–9172.
[9] J. Wu, A. Gross, H. Yang, Nano Lett. 11 (2011) 798–802.
[10] W. Yu, M.D. Porosoff, J.G. Chen, Chem. Rev. 112 (2012) 5780–5817.
[11] C. Koenigsmann, A.C. Santulli, K. Gong, M.B. Vukmirovic, W.-p. Zhou, E. Sutter, S.S. Wong, R.R. Adzic, J. Am. Chem. Soc. 133 (2011) 9783–9795.

[12] Y. Kang, X. Ye, J. Chen, Y. Cai, R.E. Diaz, R.R. Adzic, E.A. Stach, C.B. Murray, J. Am. Chem. Soc. 135 (2012) 42–45.
[13] B.N. Wanjala, J. Luo, R. Loukrakpam, B. Fang, D. Mott, P.N. Njoki, M. Engelhard, H.R. Naslund, J.K. Wu, L. Wang, Chem. Mater. 22 (2010) 4282–4294.
[14] Y. Yamauchi, A. Tonegawa, M. Komatsu, H. Wang, L. Wang, Y. Nemoto, N. Suzuki, K. Kuroda, J. Am. Chem. Soc. 134 (2012) 5100–5109.
[15] W. Zhang, J. Yang, X. Lu, ACS Nano 6 (2012) 7397–7405.
[16] Z. Peng, H. You, H. Yang, Adv. Funct. Mater. 20 (2010) 3734–3741.
[17] J. Greeley, I. Stephens, A. Bondarenko, T.P. Johansson, H.A. Hansen, T. Jaramillo, J. Rossmeisl, I. Chorkendorff, J.K. Nørskov, Nat. Chem. 1 (2009) 552–556.
[18] J. Wu, J. Zhang, Z. Peng, S. Yang, F.T. Wagner, H. Yang, J. Am. Chem. Soc. 132 (2010) 4984–4985.
[19] V.R. Stamenkovic, B. Fowler, B.S. Mun, G. Wang, P.N. Ross, C.A. Lucas, N.M. Marković, Science 315 (2007) 493–497.
[20] A.X. Yin, X.Q. Min, Y.W. Zhang, C.H. Yan, J. Am. Chem. Soc. 133 (2011) 3816–3819.
[21] X. Huang, E. Zhu, Y. Chen, Y. Li, C.Y. Chiu, Y. Xu, Z. Lin, X. Duan, Y. Huang, Adv. Mater. 25 (2013) 21–26.
[22] L. Wang, Y. Yamauchi, J. Am. Chem. Soc. 135 (2013) 16762–16765.
[23] R.J. White, R. Luque, V.L. Budarin, J.H. Clark, D.J. Macquarrie, Chem. Soc. Rev. 38 (2009) 481–494.
[24] G. Prieto, J. Zečević, H. Friedrich, K.P. de Jong, P.E. de Jongh, Nat. Mater. 12 (2012) 34–39.
[25] S.H. Joo, J.Y. Park, C.-K. Tsung, Y. Yamada, P. Yang, G.A. Somorjai, Nat. Mater. 8 (2008) 126–131.
[26] X.Y. Yang, Y. Li, G. Van Tendeloo, F.S. Xiao, B.L. Su, Adv. Mater. 21 (2009) 1368–1372.
[27] L. Qian, X. Lv, Y. Ren, H. Wang, G. Chen, Y. Wang, J. Shen, J. Chromatgr. A 1322 (2013) 81–89.
[28] J.B. Joo, P. Kim, W. Kim, J. Yi, Catal. Today 131 (2008) 219–225.
[29] S. An, J.H. Park, C.H. Shin, J. Joo, E. Ramasamy, J. Hwang, J. Lee, Carbon 49 (2011) 1108–1117.
[30] D. Kim, S. Hong, Y. Kim, K. Lee, J. Aerosol Sci. 37 (2006) 1781–1787.
[31] P. Schmidt-Winkel, W.W. Lukens, P. Yang, D.I. Margolese, J.S. Lettow, J.Y. Ying, G.D. Stucky, Chem. Mater. 12 (2000) 686–696.
[32] J. Lee, K. Sohn, T. Hyeon, J. Am. Chem. Soc. 123 (2001) 5146–5147.
[33] H. Li, Q. Xin, W. Li, Z. Zhou, L. Jiang, S. Yang, G. Sun, Chem. Commun. 23 (2004) 2776–2777.
[34] S.J. Gregg, K.S.W. Sing, Adsorption, Surface Area and Porosity, Academic Press, London, UK, 1982.
[35] Z. Nie, A. Petukhova, E. Kumacheva, Nat. Nanotechnol. 5 (2009) 15–25.
[36] X.Y. Yang, A. Leonard, A. Lemaire, G. Tian, B.L. Su, Chem. Commun. 47 (2011) 2763–2786.
[37] B.L. Su, C. Sanchez, X.Y. Yang, Hierarchically Structured Porous Materials, Wiley-VCH, Weinheim, Germany, 2012.
[38] L.H. Chen, X.Y. Li, G. Tian, Y. Li, J.C. Rooke, G.S. Zhu, S.L. Qiu, X.Y. Yang, B.L. Su, Angew. Chem. Int. Ed. 50 (2011) 11156–11161.
[39] X.Y. Yang, G. Tian, L.H. Chen, Y. Li, J.C. Rooke, Y.X. Wei, Z.M. Liu, Z. Deng, G. Van Tendeloo, B.L. Su, Chem. Eur. J. 17 (2011) 14987–14995.
[40] X.Y. Yang, Z.Q. Li, B. Liu, A. Klein-Hofmann, G. Tian, Y.F. Feng, Y. Ding, D. Su, F.S. Xiao, Adv. Mater. 18 (2006) 410–414.
[41] J. Lin, S. Wang, P. Huang, Z. Wang, S. Chen, G. Niu, W. Li, J. He, D. Cui, G. Lu, ACS Nano 7 (2013) 5320–5329.
[42] F.d.r. Blanc, M. Leskes, C.P. Grey, Acc. Chem. Res. 46 (2013) 1952–1963.

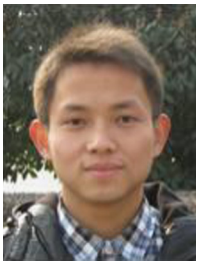

Jie Ying is currently a Ph.D. student in the Laboratory of living materials under the supervision of Prof. Dr. Bao-Lian Su and Prof. Dr. Xiao-Yu Yang from the Wuhan University of Technology, China. His current work includes design and synthesis of nanocomposites, catalysis, and self-assembly.

Xiao-Yu Yang received his Ph.D. from Jilin University (co-educated at the University of Namur, Belgium). In 2007, he held a postdoctoral position at the University of Namur with Professor Bao-Lian Su working on hierarchically porous materials. He is currently a "Chargé de Recherches" of the F.N.R.S. (National Foundation of Scientific Research). He got an honour of "Chutian scholar" at Wuhan University of Technology in 2010. His research is aimed at new synthesis pathways towards novel porous systems, catalysts, bio-nanoreactors, bio-inspired materials and biofuel cells.

Zhi-Yi Hu received his Master of Engineering degree in Materials Science from the Wuhan University of Technology in 2012. He is currently Ph.D. candidate in the physics department of the University of Antwerp and working at the EMAT (Electron Microscopy for Materials Science) research group. His research focuses on advanced transmission electron microscopy for materials, including HR-TEM, HR-STEM, STEM-EDX, STEM-EELS and 3D electron tomography.

Shi-Chun Mu received his B.S. degree from Jilin University and Ph.D. degree from Chinese Academy of Sciences, China, in 1995 and 2001 respectively. Now he is working as a Professor at State Key Laboratory of Advanced Technology for Materials Synthesis and Processing, Wuhan University of Technology. His research focuses on nanocarbon materials and PEM fuel cell and power lithium ion battery materials and related devices.

Christoph Janiak received his Ph.D. degree from Berlin Institute of Technology in 1987. Currently he is the full Professor (Chair) for Bioinorganic Chemistry and Catalysis in Heinrich-Heine-Universität Düsseldorf. He mainly works on metal-organic frameworks (MOFs), coordination polymers, chirality, supramolecular interactions, synthesis and catalysis of metal nanoparticles and metal nanoparticles in ionic liquids.

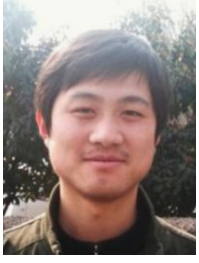

Wei Geng is currently a Ph.D. student in the Laboratory of living materials under the supervision of Prof. Dr. Bao-Lian Su and Prof. Dr. Xiao-Yu Yang from the Wuhan University of Technology, China. His current work includes design and synthesis of nanocomposites, porous materials, biomaterials and catalysis.

Mu Pan received his M.S. degree from Shanghai Jiao Tong University and Ph.D. degree from Wuhan Unverisity of Technology in 1988 and 1999 respectively. He is now a Professor at State Key Laboratory of Advanced Technology for Materials Synthesis and Processing, Wuhan University of Technology. He mainly works on polymer polymer electrolyte, proton exchange membrane fuel cell and new energy materials.

Xiaoxing Ke received her Ph.D. degree in Physics from the University of Antwerp in 2010. She is currently a postdoc researcher at EMAT, University of Antwerp, Belgium. Her research interests are focused on nanostructured materials and interface characterization using advanced electron microscopy, including HRTEM, HRSTEM, in-situ TEM and 3D electron tomography.

Gustaaf Van Tendeloo is a professor at the University of Antwerp, director of EMAT and head of the "NANO Center of Excellence" at the University of Antwerp. His research interests are focused on advanced electron microscopy for the fine structure of interfaces, nanostructures, mesoporous materials and modulated structures.

Bao-Lian Su is a member of the Royal Academy of Belgium (class of science). He is currently a Full Professor of Chemistry, Director of the Research Centre for Nanomaterials Chemistry and the Laboratory of Inorganic Materials Chemistry, Namur, Belgium. His is an "Expert of the State" in the frame of Chinese Central Government program of "Thousands Talents" and "Changjiang Professor" located at Wuhan University of Technology, China. His current research fields include the synthesis, the property study and the molecular engineering of organized, hierarchically porous and bio-inspired materials, biomaterials, living materials, nanotechnology, biotechnology, information technology, cell therapy and biomedical applications.